Clinical Cancer Research

Efficient Mitochondrial Glutamine Targeting Prevails Over Glioblastoma Metabolic Plasticity

Kristell Oizel[1], Cynthia Chauvin[1,12], Lisa Oliver[1,2,11,12], Catherine Gratas[1,2,11], Fanny Geraldo[1], Ulrich Jarry[1,12], Emmanuel Scotet[1,12], Marion Rabe[1], Marie-Clotilde Alves-Guerra[3,4,5], Raluca Teusan[6], Fabien Gautier[1,7], Delphine Loussouarn[1,2], Vincent Compan[8,9], Jean-Claude Martinou[10], François M. Vallette[1,7,11,12], and Claire Pecqueur[1,11,12]

Abstract

Purpose: Glioblastoma (GBM) is the most common and malignant form of primary human brain tumor in adults, with an average survival at diagnosis of 18 months. Metabolism is a new attractive therapeutic target in cancer; however, little is known about metabolic heterogeneity and plasticity within GBM tumors. We therefore aimed to investigate metabolic phenotyping of primary cultures in the context of molecular tumor heterogeneity to provide a proof of concept for personalized metabolic targeting of GBM.

Experimental Design: We have analyzed extensively several primary GBM cultures using transcriptomics, metabolic phenotyping assays, and mitochondrial respirometry.

Results: We found that metabolic phenotyping clearly identifies 2 clusters, GLN^{High} and GLN^{Low}, mainly based on metabolic plasticity and glutamine (GLN) utilization. Inhibition of glutamine metabolism slows the *in vitro* and *in vivo* growth of GLN^{High} GBM cultures despite metabolic adaptation to nutrient availability, in particular by increasing pyruvate shuttling into mitochondria. Furthermore, phenotypic and molecular analyses show that highly proliferative GLN^{High} cultures are $CD133^{neg}$ and display a mesenchymal signature in contrast to $CD133^{pos}$ GLN^{Low} GBM cells.

Conclusions: Our results show that metabolic phenotyping identified an essential metabolic pathway in a GBM cell subtype, and provide a proof of concept for theranostic metabolic targeting. *Clin Cancer Res; 23(20); 6292–304.* *©2017 AACR.*

Introduction

Glioblastoma (GBM), the highest grade of gliomas, is the most common and malignant form of primary human brain tumors in adults with an average survival at diagnosis of about 18 months (1). The current standard of care for patients includes tumor resection followed by radiotherapy with concomitant and adjuvant chemotherapy with temozolomide (TMZ; ref. 1). In addition to their diffuse and infiltrative nature making complete resection impossible, GBM are histologically and molecularly very diverse, exhibiting strong heterogeneity between patients as well as within individual tumors, limiting the response to therapy and leading to systematic recurrence (2–4). Tumor heterogeneity is a well-recognized hallmark of solid tumors and plays a crucial role in tumor growth, metastasis, angiogenesis, and tumor resistance. Numerous publications report that the poor response of GBM to treatment as well as tumor recurrence could be mediated by the persistence of a rare population of cells similar to stem cells that have been termed "cancer stem cells" (CSC). Thus, complete recovery from GBM would involve eradication of this population.

The singular glycolytic metabolism of tumor cells, also shared by CSC (5), was recently included as one of the hallmarks of cancer cells (6) supporting the proposition that compounds altering cell metabolism could be exploited as new therapeutic approaches or synergistic improvements to actual therapies. Indeed, to fulfill the large amounts of both biomass precursors and ATP production required by tumor proliferation and invasion, tumor cells reprogram their metabolism by increasing their glycolytic and anaplerotic fluxes. This glycolytic switch, also known as the Warburg effect, drives several anabolic pathways supporting growth and proliferation of tumor cells. Furthermore, because glucose is converted to lactate at the expense of its mitochondrial oxidation, cancer cells need glutamine (GLN) to drive mitochondrial metabolism (7). Besides providing carbon for TCA-cycle anaplerosis, glutamine

[1]CRCINA, INSERM, Université de Nantes, France. [2]Centre Hospitalier-Universitaire (CHU) de Nantes, Nantes, France. [3]Inserm, U1016, Institut Cochin, Paris, France. [4]CNRS, UMR 8104, Paris, France. [5]Université Paris Descartes, Sorbonne Paris Cité, Paris, France. [6]Institut du thorax, INSERM, CNRS, UNIV Nantes, Nantes, France. [7]Institut de Cancérologie de l'Ouest, René Gauducheau, St Herblain, France. [8]Institute of Functional Genomics, Labex ICST, CNRS, UMR 5203, University of Montpellier, Montpellier, France. [9]INSERM U1191, Montpellier, France. [10]Department of Cell Biology, University Geneva, Geneva, Switzerland. [11]Equipe labellisée Ligue contre le Cancer. [12]Labex IGO "Immunotherapy, Graft, Oncology."

Note: Supplementary data for this article are available at Clinical Cancer Research Online (http://clincancerres.aacrjournals.org/).

K. Oizel and C. Chauvin contributed equally to the article.

Corresponding Authors: Claire Pecqueur, CRCINA, INSERM, University, de Nantes, France, 8 quai Moncousu BP 70721, 44007 Nantes, Frances. Phone: 332 0228 080325; Fax: 332 0228 080204; E-mail: claire.pecqueur@univ-nantes.fr; François M. Vallette, IRSUN, 8 quai moncousu, BP70721, 44007 Nantes, France. E-mail: francois.vallette@univ-nantes.fr

doi: 10.1158/1078-0432.CCR-16-3102

Translational Relevance

Glioblastoma (GBM) is one of the most common and malignant forms of primary human brain tumor in adults, with a survival of 18 months even under very aggressive treatments. The clinical characteristics and prognosis of patients with GBM are not accurately reflected by histological classification. In this work, through a combination of transcriptomic and metabolomic analyses, we show that metabolic phenotyping has identified an Achilles' heel in the more resistant GBM subtype to therapy and mirrored molecular signatures. Our study brings new insight into the potential therapeutic use of metabolic inhibitors and provides a proof of concept for theranostic metabolic targeting in the context of GBM. Stratification of future clinical trials based on these molecular and metabolic subsets should improve the development of effective therapies and uncover new predictive markers.

can also supply α-ketoglutarate to support amino acid catabolism, be a direct nitrogen donor for nucleotide biosynthesis (8), and is implicated in redox balance (9). Despite their avidity for nutrients, cancer cells often encounter conditions of nutrient scarcity *in vivo*, which usually triggers further metabolic adaptations (10–12) based on the tumor microenvironment. Interestingly, previous studies have shown that, for some tumors such as diffuse large B-cell lymphoma (DLBCL), subsets can be discriminated based on metabolic fingerprints (13). In fact, the emergence of personalized molecular approaches opens the path to novel diagnosis and therapeutic options, including the use of metabolic inhibitors. Indeed, drugs targeting glutaminase 1 (GLS1) are currently being explored as therapies in breast cancer (14).

In our study, we show that primary cultures derived from patient tumors exhibit metabolic heterogeneity and plasticity. Interestingly, this metabolic hierarchism was mirrored by molecular and cellular heterogeneity and pointed out glutamine as a potential therapeutic target in a specific GBM subset.

Materials and Methods

Unless stated otherwise, all cell culture material was obtained from Life Technologies and chemicals were from Sigma-Aldrich.

Human GBM tumor cells

Primary GBM cultures were derived after mechanical dissociation from high-grade glioma operated on 14 patients. All procedures involving human participants were in accordance with the ethical standards of the ethic national research committee and with the 1964 Helsinki declaration and its later amendments or comparable ethical standards. Informed consent was obtained from all individual participants included in this study. Primary GBM cells were cultured in defined medium (DMEM/HAM-F12, 2 mmol/L L-glutamine, N2 and B27 supplement, 2 μg/mL heparin, 20 ng/mL EGF and 25 ng/mL bFGF, 100 U/mL penicillin and 100 μg/mL streptomycin). All the experiments with primary GBM cells were performed at early passages. The U87-MG cell line was obtained from ATCC and cultured in DMEM 5 mmol/L glucose supplemented with 10% FCS, 2 mmol/L L-glutamine and 100 U/mL penicillin, and 100 μg/mL streptomycin. Cells were checked for *mycoplasma* regularly. Metabolic inhibitors, EGCG (110 μmol/L), DON (50 μg/mL), BPTES (10 μmol/L), and 2-DG (5 mmol/L), were added to the culture media when required, unless stated otherwise.

Cell proliferation

Cell counts and viability were performed using the Countess optics and image automated cell counter (Life Technologies). Cells were mixed with Trypan blue (50/50) and loaded into a Countess chamber slide. The image analysis software was used to automatically analyze the acquired cell images from the sample to give cell count and viability. Data were plotted as the number of viable cells for cell proliferation or compared with proliferation in control condition for relative proliferation. Concentration of 2-DG inhibiting 50% cell proliferation (IC_{50}) was extrapolated from cell proliferation assessed 48 hours after the addition of increasing amounts of 2-DG using the alamar blue dye following the manufacturer's instructions.

Transcriptomic analysis

Samples provided as section of areas immediately adjacent to the region used for the histopathological diagnosis were mechanically dissociated, cultured in define media for less than 2 passages, and frozen. Total RNA was obtained using the RNeasy mini kit (Qiagen) according to the manufacturer's instructions. RNA quality was verified with the Bioanalyzer System (Agilent Technologies) using the RNA Nano Chip. RNA (1.5 μg) was processed and hybridized to the Genechip Human Genome U133 Plus 2.0 Expression array (Affymetrix), which contains over 54,000 probe sets analyzing the expression levels of over 47,000 transcripts and variants. This roughly corresponds to 29,500 distinct Unigene identifiers. The processing was done according to the recommendations of the manufacturer. The raw signals of each probes for all the arrays where normalized against a virtual median chip (median raw intensity per row) using a local weighted scattered plot smoother analysis. The data were filtered to remove probes with low intensity values by sample category in order to keep the signature of little class of sample. The hierarchical clustering used to detect groups of correlated genes, supported by a statistical method (limma) to detect differential expression among biological conditions, was computed on median-gene-centered and log-transformed data using average linkage and uncentered correlation distances with the Cluster program (15). Functional annotations of gene clusters and differential expressed genes were performed using GoMiner software (16) and the Gene Ontology database (17). Raw and normalized data have been deposited in the GEO database under accession number (GSE83626).

RT-qPCR

Quantitative real-time PCR assays were performed in triplicate using the real-time thermal cycler qTOWER (Analytic Jena) after total RNA isolation and reverse transcription. Three housekeeping genes were amplified and used to normalized with other gene transcripts. Relative transcript expression was calculated compared with the mean of all primary GBM for the

corresponding gene. The list of primers used is indicated in Supplementary Table S2.

Metabolic analyses

Analysis of various substrates utilization was performed using PM-M1 and PM-M2 Biolog microplates, coated with different oxidizable carbon sources in various wells, following the manufacturer's instructions (18). Briefly, cells (30×10^3/well) were plated on Biolog microplate for 24 hours in IFM1 media at 37°C and under 5% CO_2 allowing the cells to use up residual carbon-energy sources. Metabolic activity was then recorded spectrophotometrically for 24 hours by adding a Redox Dye Mix (Dye A). Metabolic activity value was obtained after deduction of the metabolic background obtained from negative controls (no substrate in the well). Glucose was measured in cell medium using the Roche diagnostic kit on a Cobas 8000 (Roche Diagnostics) as described previously (19). Amino acids in the culture medium were labeled using a TRAQ (ABSciex) kit and measured by LC-MS/MS with norleucine and norvaline as internal controls. Concentrations were calculated using the software Analyst (ABSciex). Glucose, glutamine, alanine, and aspartate consumption, and production was calculated as the amount present in cell medium after 48 hours of culture minus the initial amount, and reported to 1×10^6 cells. Metabolic dependency to glucose was assessed either by replacing glucose (17.5 mmol/L) by galactose (17.5 mmol/L) in cell media progressively over 4 weeks or with dose–response curves using 2-deoxyglucose (2-DG). IC_{50} of 2-DG was extrapolated from the mean of 3 independent curves using PRISM6 software.

Mitochondrial oxygen consumption (OCR) and extracellular acidification rate (ECAR), reflect of glycolysis, were measured in non-buffered medium supplemented with glucose (5 mmol/L), pyruvate (1 mmol/L), and glutamine (2 mmol/L) using an XF24 Analyzer (Seahorse Bioscience). Specific mitochondrial respiration fueled with either glucose (ΔOCR_{GLC}) or glutamine (ΔOCR_{GLN}) was determined by the difference of the mean of the 3 values of OCR in the absence of substrate and the mean of the 4 values of OCR after injection of the substrate. Glucose was injected to a final concentration of 5 mmol/L and glutamine 2 mmol/L. Basal OCR was measured in non-buffered medium containing glutamine (2 mmol/L) or pyruvate (1 mmol/L) to calculate respectively ΔOCR_{GLC} and ΔOCR_{GLN}.

BRET measurement

Cells were transfected with empty vector, pWPT-MPC1-Venus, pWPT-MPC2-luciferase 8 or both (ratio 1:1) using Lipofectamine-3000 (Life Technologies) following the manufacturer's instructions. Two days after transfection, cells were plated (3×10^4 cells/well) in white 96-well plates and BRET was recorded 24 hours later (20). For BRET measurement in the presence of EGCG, 48 hours after transfection, cells were plated at 15,000 cells/well, grown for 6 days in the presence of EGCG (110 μmol/L) and processed as before. Results were expressed as mean ± SD.

FACS analysis and immunochemistry

Primary GBM cells were dissociated, washed, and incubated 30 minutes with the primary antibody CD133-APC. Data acquisition was performed on a FACS Calibur (Becton Dickinson) and analyzed using the FlowJo V.10 software. For immunochemistry, brains were collected from euthanized mice, fixed (PBS, 4% paraformaldehyde, PBS-PFA), embedded in paraffin wax and serially sectioned. Paraffin-embedded brain sections were saturated with 2% BSA (Sigma) and then with rabbit anti-human CD3 (Dako, Agilent Technologies) or rabbit anti-human anti-MHC class I Ab (clone EPR1394Y; Abgent). Revelation was performed using polymer histofine anti-rabbit coupled to HRP (Microm Microtech France) and the DAB detection system (Leica), and slides were scanned using nanoZoomer 2.0 HT (Hamamatsu Photonics K.K., Hamamatsu, Japan).

Orthotopic injections of human primary cells in NSG mice

NSG (*NOD.Cg-Prkdcscid Il2rgtm1Wjl/SzJ*) mice (Charles River Laboratories) were bred in the animal facility of the University of Nantes (UTE, SFR F. Bonamy) under SPF status and used at age 6 to 12 weeks, according to institutional guidelines (Agreement # 00186.02; Regional ethics committee of the Pays de la Loire, France). Orthotopic injections of human GBM cells (10^4 in 2 μL PBS), pretreated or not with EGCG, were performed using a stereotactic frame (Stoelting) at 2 mm on the right of the medial suture and 0.5 mm in front of the bregma, depth: 2.5 mm. Animals were observed daily and euthanized when characteristic symptoms occurred, such as reduced mobility and significant weight loss.

Isolation and enrichment of tumor cells from mouse brains

For GBM cell isolation, cells were collected from the mouse brains by using the human tumor dissociation kit (Miltenyi Biotec) followed by a discontinuous 30/70% isotonic Percoll gradient (Sigma-Aldrich) and isolated using anti-human HLA mAb (clone w6/32; BioXCell) and the "CELLectionTM Pan Mouse IgG Kit" (Life Technologies), accordingly to the manufacturer's instructions. Isolated cells were then used for *in vitro* metabolic analyses.

Statistical analysis

Data were analyzed and statistical analyses were performed using GraphPad Prism 6.00 (GraphPad Software). Data points are expressed as mean ± SD unless otherwise indicated. *, $P < 0.05$; **, $P < 0.01$; ***, $P < 0.001$. Hierarchical clustering using metabolic phenotyping assay (data at 1245 minutes) and RT-qPCR data (ΔCt after normalization) were realized using XLSTAT software.

Results

Metabolic phenotype microarray of primary GBM cultures

Tumor samples from 14 GBM patients, mechanically dissociated and cultured in define media, grew usually as spheres (Table 1; Supplementary Fig. S1A). These spheres were further characterized using light-sheet microscopy allowing deep light penetration and exhibited a central necrotic core, similar to that observed in high-grade tumors in patients (Supplementary Fig. S1B). The metabolic profile of 8 primary GBM cultures was next investigated using the Biolog metabolic phenotype technology. This assay measured over time the generation of the high-energy molecule NADH from various metabolic pathways, starting from unique carbon, nitrogen, or phosphate sources, allowing the subsequent reduction of a redox dye (Fig. 1A). All tested GBM cells were able to take up glucose and to convert it into NADH, through glycolysis and TCA cycle (Supplementary Fig. S2A). Whereas early kinetics differed from one GBM culture to another, NADH formation reached a

Table 1. Primary cultures characteristics

	Tumor	Tumor IDH status	Glutamine metabolism	Molecular subtype	Mice survival
1	GBM IV	Wild-type	High	Mesenchymal	32 days
2	GBM IV	Wild-type	Low	Proliferative	n/a
3	GBM IV	Wild-type	Low	Proliferate	>6 mo
4	GBM IV	Wild-type	High	Mesenchymal	>6 mo
5	GBM IV	Wild-type	Low	Proneural	4.9 mo
6	GBM IV	Wild-type	Low	Proliferative	5.1 mo
7	GBM IV	Wild-type	Low	Proneural	n/a
8	GBM IV	Wild-type	High	Mesenchymal	n/a
10	GBM IV	Wild-type	Low	Proliferative	43 days
11	GBM IV	Wild-type	High	Mesenchymal	4.5 mo
12	GBM IV	Wild-type	High	Mesenchymal	>6 mo
13	GBM IV	Wild-type	Low	Proliferate	>6 mo
14	GBM IV	Wild-type	Low	Proliferate	>6 mo
16	GBM IV	Wild-type	Low	Proliferate	>6 mo

NOTE: Grade and IDH status determined after immunohistological studies are indicated for each tumor sample leading to a primary culture. Metabolic classification (GLN^{High} vs. GLN^{Low}) as well as molecular classification are indicated for each primary culture. Mice survival after orthotopic injection of primary cultures was recorded and indicated for all primary cultures tested.

plateau after 6 hours in all GBM cells with no significant difference between cultures. Of note, all GBM cells were able to generate NADH from a variety of hexoses, some alcohols, nucleosides, and TCA cycle intermediates (Supplementary Table S1). Interestingly, unsupervised clustering of the overall metabolic profiling resulted in a dendrogram clearly separating the samples into 2 clusters (Fig. 1B). In particular, primary GBM-4, -12, -1, -11 cultures were grouped in a cluster (called hereafter GLN^{High}) with globally a wider ability to use different metabolic sources to generate NADH. Importantly, these cells were able to take up glutamine (Fig. 1C) and convert it into NADH (Fig. 1D), in the absence of other nutrients, in contrast to the GBM cells in the second cluster (called hereafter GLN^{Low}). To strengthen these observations, 6 other primary cultures were analyzed for glutamine consumption and NADH generation (Supplementary Fig. S2B). Similarly, primary GBM-8 culture exhibited strong glutamine consumption correlated with high NADH generation whereas the other 5 primary cultures consumed little glutamine and generated less NADH. Following from these observations, we classified GBM-1, -4, -8, -11, and -12 in the GLN^{High} cluster and the other GBM cultures in the GLN^{Low} cluster (Table 1).

Distinct utilization of glutamine between the 2 clusters

Once internalized, glutamine is converted by mitochondrial glutaminase to glutamate, which is further catabolized to α-ketoglutarate to generate ATP through the production of reducing equivalents NADH and FADH2 via the TCA cycle (Fig. 2A). Glutamate is converted to α-ketoglutarate either through the glutamate dehydrogenase (GLUD) leading to ammonia generation, or through several aminotransferases, where nitrogen is transferred to generate other amino acids, in particular aspartate or alanine. In order to investigate the fate of glutamine in GBM cells, aspartate and alanine concentrations as well as expression of several glutamine transporters and enzymes involved in glutamine metabolism were analyzed. First, while there were minor differences in aspartate production among GBM cultures (Supplementary Fig. S2C), the concentration of alanine in culture media was greatly increased in GLN^{High} cells compared with GLN^{Low} cells (Fig. 2B). Furthermore, all GLN^{High} cells had a higher RNA level of the glutamine transporter SLC1A5, glutaminase (GLS), and mitochondrial and cytosolic aminotransferase (GOT1 and 2; Supplementary Fig. S3A). No difference in the expression of GPT1 nor GLUD was observed between GLN^{High} and GLN^{Low} cells (Supplementary Fig. S3A). In addition, with the exception for GBM-9, c-MYC, a master regulator of genes involved in glutamine metabolism, was similarly expressed in all GBM cultures (Supplementary Fig. S3B). To investigate further glutamine metabolism, mitochondrial respiration based on glutamine was measured using the Seahorse technology. Two different profiles of oxygen consumption (OCR) were observed after glutamine addition (Fig. 2C). GBM-1 culture (GLN^{High}) increased its mitochondrial respiration in the presence of glutamine (ΔOCR_{GLN}) while GBM-10 (GLN^{Low}) showed no difference. Interestingly, all GLN^{Low} cultures, with the exception of GBM-7 cells, did not use glutamine to sustain mitochondrial respiration, while all GLN^{High} cultures exhibited a significant increase in mitochondrial respiration after glutamine addition (Fig. 2D). Similar experiments were performed to investigate whether GLN^{Low} cells used glucose as a source for mitochondrial respiration (Fig. 2D). As expected, OCR was mainly sustained through glycolytic pyruvate in GLN^{Low} cells. Of note, the addition of ΔOCR_{GLN} and ΔOCR_{GLC} was only about 45%, clearly suggesting that other substrates fueled mitochondrial respiration besides glucose and glutamine.

Altogether, these results show that GLN^{Low} cells are characterized by a limited ability to use glutamine while GLN^{High} cells metabolize glutamine to sustain their mitochondrial respiration and to generate alanine.

GLN^{Low} GBM cultures require glucose for their proliferation

Besides analyzing the expression of enzymes involved in glutamine metabolism, the level of glucose transporters as well as glycolytic enzymes was evaluated in GBM cultures. No differences were observed in glucose transporters expression between the two groups (data not shown). Expression of both lactate dehydrogenase (LDHA) and pyruvate dehydrogenase (PDHA1), 2 enzymes involved in the conversion of glycolytic pyruvate into either cytosolic lactate or mitochondrial acetyl-CoA, respectively, was highly expressed in GLN^{Low} GBM cultures (Supplementary Fig. S3C). Furthermore, these cells also exhibited a higher RNA level of the M-isoform of pyruvate kinase (PKM), which catalyzes the last but rate-limiting step of glycolysis (Supplementary Fig. S3C). These results prompted

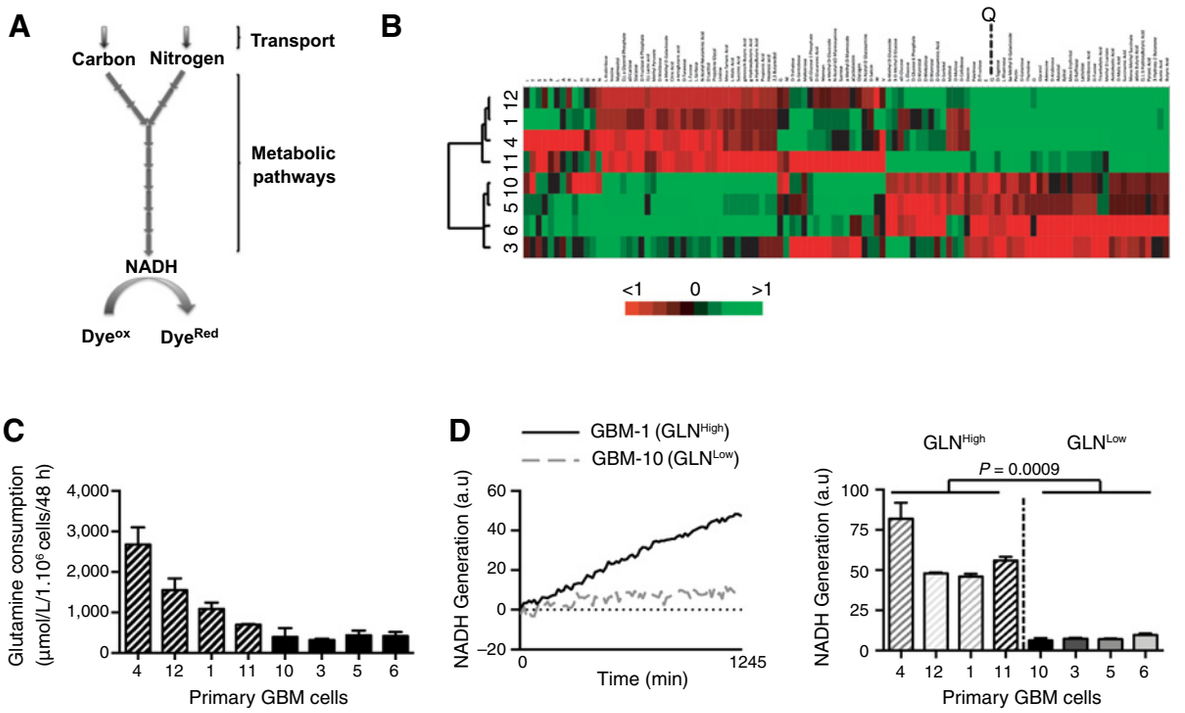

Figure 1.

Metabolic phenotyping of primary GBM cultures. **A,** Schematic Biolog principle. **B,** Unsupervised hierarchical clustering of primary GBM cultures using the metabolic phenotyping results. **C,** Glutamine consumption of 14 primary GBM cells over 48 hours and expressed for 1×10^6 cells. The 2 groups identified in **B** are indicated as dashed bars and black bars. **D,** NADH generation from glutamine metabolism of primary GBM cultures. Left, NADH generation over time of GBM-1 (black line) and GBM-10 (gray line) cultures (mean of triplicate). Right, NADH generation at 1,245 minutes for 8 primary GBM cultures. GLN^{High} cells are indicated as dashed bars and GLN^{Low} cells as plain bars. ($n = 3$; t test analysis).

a further characterization of glucose metabolism in GBM cultures. First, the addition of glucose in the metabolic phenotype assay significantly increased glutamine-dependent NADH generation in GLN^{High} cells in contrast to GLN^{Low} cells (Fig. 3A). Second, GLN^{Low} cells relied more on glycolysis compared with GLN^{High} cells as shown by the IC_{50} of 2-deoxyglucose [2-DG; mean ± SD: GLN^{High} 78 ± 24 ($n = 5$) vs. GLN^{Low} 13 ± 6 ($n = 6$)], a potent inhibitor of glycolysis (Fig. 3B). Finally, glucose dependency for proliferation of 3 GBM cultures from each group was investigated by completely replacing, in the media, glucose by galactose over 4 weeks. As expected, metabolic analysis showed that glycolysis was significantly decreased while mitochondrial respiration increased in the presence of galactose (Supplementary Fig. S4). Interestingly, GLN^{Low} cells were unable to proliferate under these conditions (Fig. 3C). In contrast, proliferation of GLN^{High} cells was not affected by the absence of glucose. Moreover, these results were confirmed in the metabolic phenotype microarray because only GLN^{High} cells were able to generate NADH directly from galactose (Supplementary Table S1).

Altogether, these results show that GLN^{Low} cells are strictly dependent to glucose while GLN^{High} cells adapt their metabolism to glucose deprivation.

EGCG inhibits cell proliferation in GLN^{High} cells

Various metabolic inhibitors of glutamine metabolism (DON, BPTES, and EGCG) were tested for their ability to inhibit cell proliferation and glutamine-sustained mitochondrial respiration. First, these compounds were tested in U87-MG cells, which recapitulated metabolic GLN^{High} cell behavior (Supplementary Fig. S5). While all inhibitors reduced cell proliferation and mitochondrial respiration in U87-MG cells, EGCG at 110 µmol/L was the most potent inhibitor of these two processes. Interestingly, this compound also significantly reduced cell proliferation in GLN^{High} cultures but had no effect on GLN^{Low} cells (Fig. 4A). Furthermore, the proliferation with EGCG was similar to that observed under glutamine-deprived conditions (Fig. 4B). All these observations led to further investigations into how EGCG altered glutamine metabolism. In all primary GLN^{High} cells, glutamine-based mitochondrial respiration was significantly reduced after a 24-hour pretreatment with EGCG (Fig. 4C). In contrast, the weak mitochondrial glutamine consumption was not affected by EGCG in GLN^{Low} cultures.

Altogether, these data suggest that EGCG inhibits cell proliferation in GLN^{High} cells through mitochondrial glutamine targeting.

EGCG induces a long-term metabolic adaptation from glutamine to glucose

To investigate the ability of GLN^{High} cells to adapt to metabolic deprivation, glucose and glutamine metabolism was investigated after 6 days of EGCG. Under these conditions, ΔOCR_{GLN} was still significantly reduced (Fig. 5A). Interestingly,

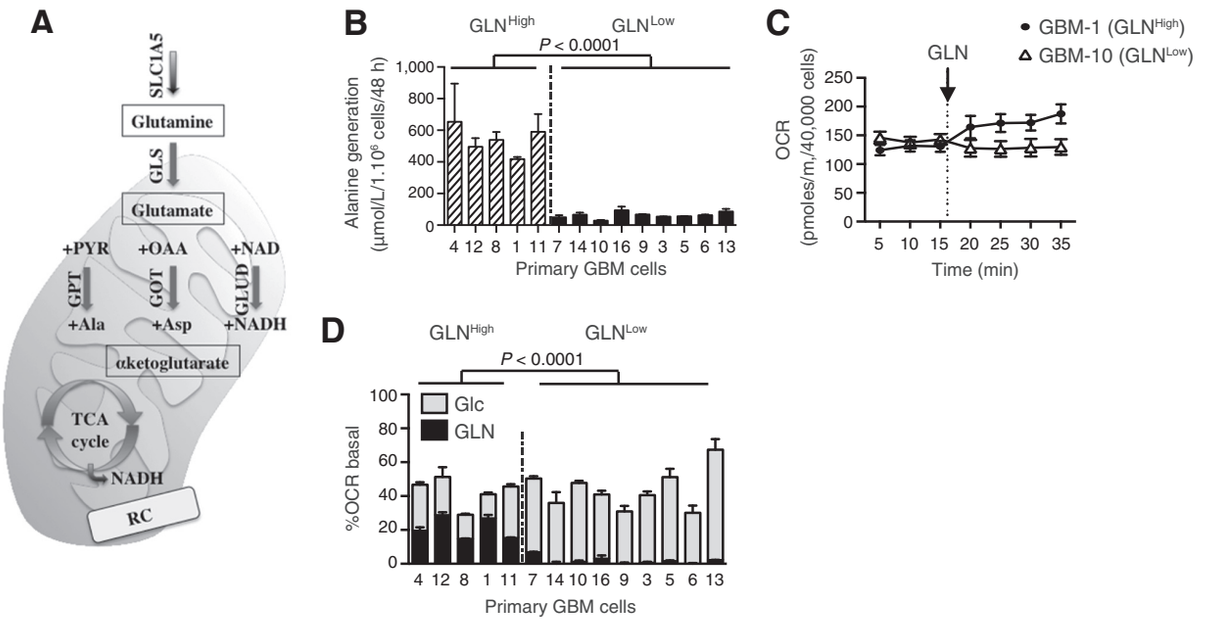

Figure 2.

Glutamine metabolism of GLN^{High} and GLN^{Low} cultures. **A,** Schematic representation of glutamine metabolism. RC, Respiratory Chain. **B,** Alanine generation of 14 primary GBM cells over 48 hours and expressed for 1×10^6 cells. GLN^{High} cells are indicated as dashed bars and GLN^{Low} cells as black bars. ($n = 3$; *t* test analysis). **C,** Oxygen consumption rate (OCR) profile of GBM-1 (GLN^{High}, black circles) and GBM-10 (GLN^{Low}, white triangles) cells (representative experiment, mean of triplicates ± SD). **D,** Mitochondrial respiration sustained by glutamine (black) or glucose (gray) in primary GBM cells. Results are expressed as the percentage of OCR after substrate addition compared with basal OCR ($n \geq 3$; *t* test analysis).

cells compensate this loss of mitochondrial supply through a metabolic shift as shown by the increased in ΔOCR_{GLC} (Fig. 5B). These results suggested that cells adapted to EGCG treatment by favoring the entry of glycolytic pyruvate into mitochondria. To confirm this hypothesis, activation of the mitochondrial pyruvate carrier (MPC) was determined by BRET using the RESPYR biosensor assay (20). We first confirmed using U87-MG cells that addition of exogenous pyruvate triggered the activation of MPC (Supplementary Fig. S6A). Then the activation of MPC was analyzed in the presence of increasing amounts of pyruvate with or without a 6-days EGCG pretreatment in U87-MG cells because these cells undergo a similar mitochondrial metabolic shift after EGCG treatment (Supplementary Fig. S6B). In control U87-MG cells, increasing amounts of pyruvate triggered the activation of MPC (Fig. 5C). When cells were pretreated with EGCG, a significantly stronger BRET signal was detected in the absence or at low concentrations of exogenous pyruvate. At higher concentrations, above 5 mmol/L, EGCG did not affect MPC activation (Fig. 5C). BRET analyses were then performed on primary cells in the absence of pyruvate (Fig. 5D). As expected, EGCG pretreatment did not affect MPC activation in GBM-10 cells, which barely used glutamine to sustain their mitochondrial respiration. However, in GBM-1 cells, EGCG significantly activated MPC in the absence of pyruvate. Altogether, these results demonstrated that EGCG triggered a metabolic shift toward glycolysis in GLN^{High} cells. Actually, this glycolytic shift triggered by EGCG should increase the glucose dependency of GLN^{High} cells. Indeed, when cell proliferation was measured in the presence of increasing amounts of 2-DG, the IC_{50} of 2-DG for GBM-1 culture was markedly reduced in the presence of EGCG (CTR 286 ± 51 mmol/L vs. EGCG 87 ± 17 mmol/L, $P < 0.01$), whereas EGCG did not affect glucose dependency in GBM-10 (CTR 11.8 ± 1 vs. EGCG 12.5 ± 1; Fig. 5E). Moreover, 2-DG IC_{50} was decreased in all GLN^{High} cultures tested and was unaffected in all GBM^{Low} cells (Fig. 5F).

EGCG reduces cell growth of GLN^{High} cells *in vivo*

Because GLN^{High} cells are able to adapt their metabolism to nutrient restriction and as a wider extent to their microenvironment, the ability of EGCG to specifically reduce the cell proliferation of GLN^{High} cells was investigated *in vivo*. All primary GBM cultures triggered the growth of a highly invasive tumor (Fig. 6A, top; and Table 1) in NSG immune-deficient mice. Most of the primary GBM cultures tested resulted in a slow growing tumor without any clinical symptoms for more than 6 months. However, some mice exhibited clinical symptoms several weeks after injection, in particular those injected with GLN^{High} GBM-1 and GLN^{Low} GBM-10 cells, associated respectively with a median survival of 30 and 59 days (Fig. 6A). These 2 primary cultures were then treated for 6 days with EGCG prior to intracranial injection. Of note, cell viability was similar in all groups (>90%), regardless of EGCG pretreatment or not. Mice survival was significantly increased when GBM-1 cells were pretreated with EGCG prior to intracranial injection, in contrast to mice injected with GBM-10 cells where EGCG had no significant effect on survival. As these cells exhibited a strong glycolytic phenotype, similar experiments were performed with the glycolytic inhibitor 2-DG. No differences were observed in mice survival in both groups whether cells were pretreated with 2-DG prior to orthotopic injection (Fig. 6A) or when 2-DG was injected three times a week intraperitoneally in tumor-bearing

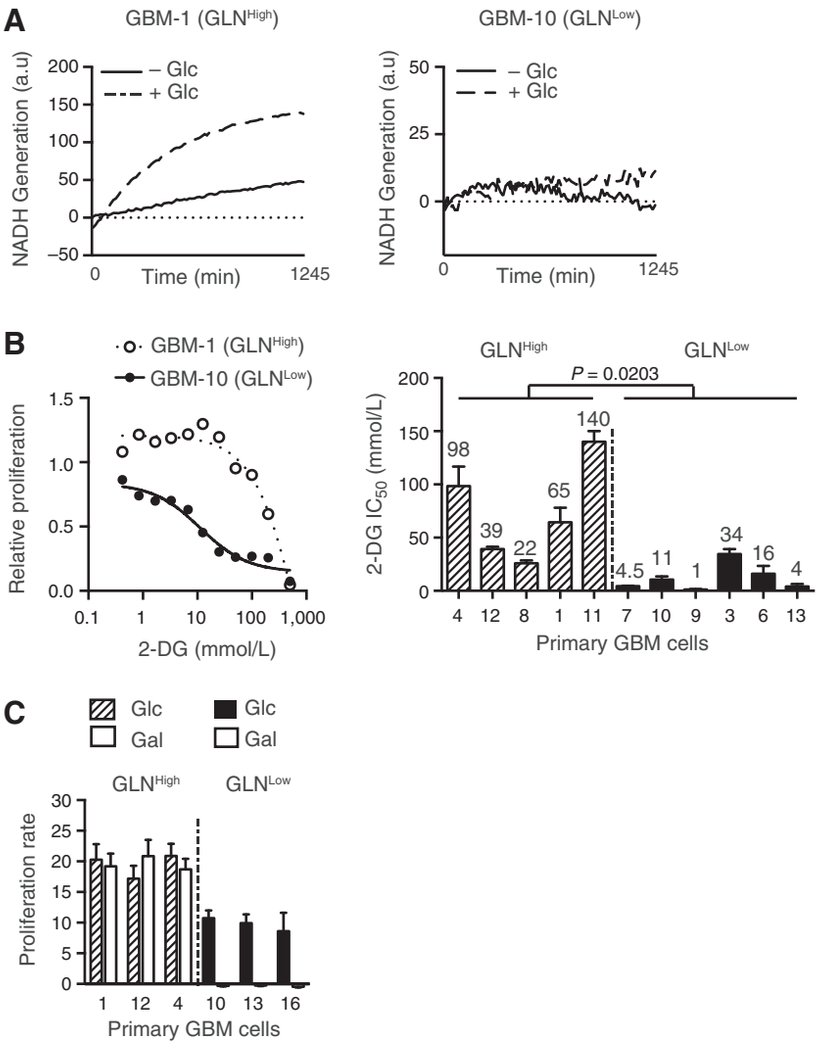

Figure 3.
Glucose dependency of GLN^{High} and GLN^{Low} cultures. **A,** NADH generation overtime from glutamine metabolism in absence (solid line) or in the presence of 0.5 mmol/L glucose (dashed line) in GLN^{High} GBM-1 (left) and GLN^{Low} GBM-10 cells (right; mean of triplicate). **B,** Glucose dependency of primary GBM cultures. Cell proliferation was assessed over 48 hours in the presence of increasing amounts of 2-DG. Dose–response curves of GLN^{High} GBM-1 and GLN^{Low} GBM-10 cells (left panel; mean of 3 independent experiments) and 2-DG IC_{50} of all primary GBM cells (right). GLN^{High} cells are indicated as dashed bars and GLN^{Low} cells as plain bars. Mean value is indicated on top of each bar (mean ± SD; $n \geq 3$, *t* test analysis). **C,** Proliferation of 3 GLN^{High} (dashed bars) and 3 GLN^{Low} (plain bars) primary GBM cells in the absence of glucose after 4 weeks of cell adaptation to galactose. Cell proliferation was assessed over time in the presence of either glucose only (black) or galactose only (white) after 72 hours by Trypan blue exclusion (mean ± SD; $n \geq 3$).

mice (data not shown). Finally, cells from control and EGCG-treated GBM-1 tumors were dissociated, enriched for tumor cells, and analyzed for their mitochondrial respiration. Interestingly, ΔOCR_{GLN} was significantly reduced in tumors arising from EGCG-pretreated cells compare with control cells, even if cells were not exposed to EGCG *in vivo* (Fig. 6B).

These results show that EGCG induced a permanent metabolic shift reducing tumor cell proliferation *in vivo*.

GLN^{High} cells are CD133^{neg} and exhibit a molecular mesenchymal signature

Finally, we investigated molecular and phenotypic differences between GLN^{High} and GLN^{Low} primary GBM cells. First, ΔOCR_{GLN} correlated with cell proliferation because all GLN^{High} cells proliferate faster than GLN^{Low} cells (Fig. 7A). Because these cultures were highly heterogeneous, the presence of CSC was further characterized using extreme limiting dilution assay (ELDA) as well as analysis of stem cell surface markers. ELDA assays showed that all primary cultures contained significant amounts of stem cells with no significant difference between the 2 culture groups (Supplementary Fig. S7A). Furthermore, no difference was observed in CD44 expression between primary cultures (Supplementary Fig. S7B). Interestingly, cells expressing the CD133 marker were easily detected in all GLN^{Low} cells but they were barely present in GLN^{High} cells (Fig. 7B). Of note, none of these primary cells exhibited an IDH1 or IDH2 mutation, or originated from an IDH-mutated tumor (Table 1). Finally, an unsupervised hierarchical transcriptomic analysis of 12 primary cultures using the most variable genes allowed a molecular discrimination between 2 groups mirroring the metabolic phenotype clustering (Fig. 7C). Gene expression profiling and subsequent combined genomic and TCGA analysis revealed that GBM can be subdivided into several main subtypes based on patient prognosis and gene expression clustering. Interestingly, hierarchical clustering using 2 different dataset probes, namely Philips (Fig. 7D) and Verhaak (Fig. 7E) molecular signatures, showed that GLN^{High} cultures correlated with the mesenchymal signature whereas all GLN^{Low} belong to one of the other GBM subtypes. To characterize the 2 primary cultures, which were not included in the transcriptomic analyses, the most discriminant genes were selected and amplified by RT-qPCR. As expected, mesenchymal GLN^{High} and GLN^{Low} cultures clustered as previously observed (Fig. 7F). Both GBM-5 and GBM-6 exhibited a non-

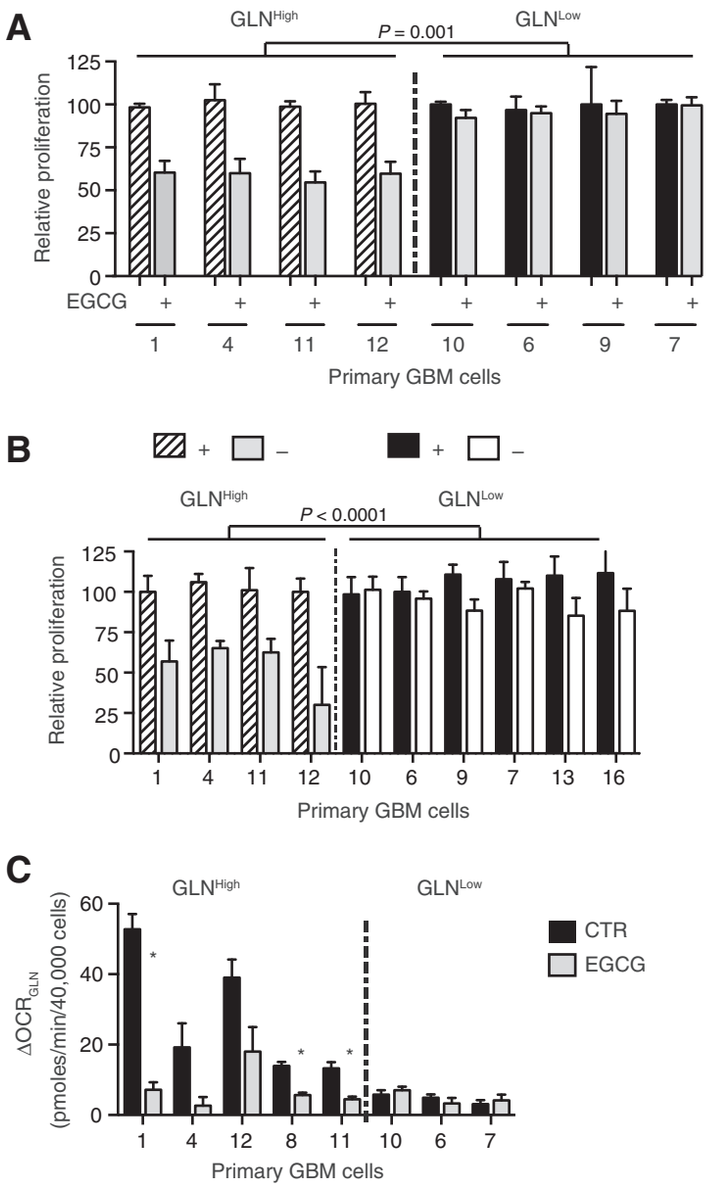

Figure 4.

EGCG slows down GLN^{High} cell proliferation and inhibits ΔOCR_{GLN}. **A,** Inhibition of proliferation in GLN^{High} cells after addition of inhibitors of glutamine metabolism. Cell proliferation was assessed by cell counting using trypan blue exclusion in primary GBM cells in the presence of 110 μmol/L EGCG after 72 hours (mean ± SD; $n \geq 3$; two-sided ANOVA). **B,** Proliferation of primary cultures in the presence or absence of glutamine. Primary GLN^{High} cells are indicated as dashed bars and GLN^{Low} cells as plain bars (mean ± SD; $n \geq 3$; two-sided ANOVA). **C,** Inhibition of mitochondrial respiration fueled with glutamine (ΔOCR_{GLN}) in primary cells. ΔOCR_{GLN} was measured in cells 24 hours after the addition of 110 μmol/L EGCG in GLN^{High} and GLN^{low} primary cells (mean ± SD; $n \geq 3$; multiple *t* test respectively).

mesenchymal signature, which was in agreement with our metabolic and phenotypic characteristics. Altogether, these results show that metabolic phenotyping closely mirrors molecular classification.

Discussion

Tumors often wire their metabolism to supply metabolic intermediates for new biomass synthesis, energy generation as well as reducing equivalent formation (21). One of the first metabolic alterations observed in tumors is an elevated glycolysis, even in presence of a sufficient oxygen supply, known as the Warburg effect. Recently, the importance of mitochondria and the utilization of alternative oxidizable substrates such as glutamine in tumor cell survival and proliferation have been clearly demonstrated (13, 22). In our study, using transcriptomics, metabolic phenotype assay and mitochondrial respirometry, we show clear metabolic distinctions between 2 clusters of primary GBM cultures. Our data show that glutamine needs and uses differ significantly between the mesenchymal GLN^{High} group, which have a huge glutamine uptake, and a second group with low GLN consumption (GLN^{Low}). Furthermore, in GLN^{High} cells, glutamine-derived glutamate is converted into α-ketoglutarate to generate ATP through the production of reducing equivalents (NADH, FADH2) and mitochondrial respiration, and to generate alanine, in contrast to GLN^{Low} cells. This metabolic difference, independent of *c-myc*, can be explained by a higher expression of several mRNA involved in glutamine metabolism such as the glutamine transporter SLC1A5, glutaminase (GLS), and glutamine aminotransferase (GOT). First, these results challenge the notion that glutamine dependency of cells *in vitro* relies mostly on the glutamine

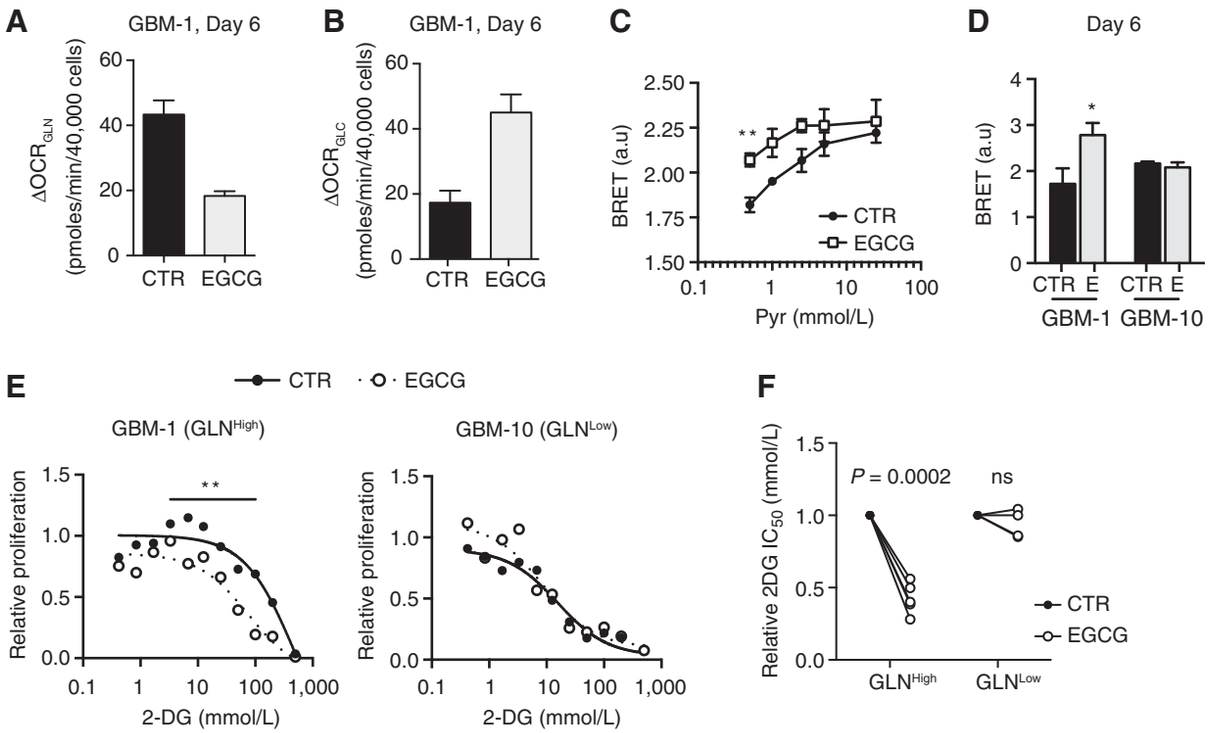

Figure 5.

Metabolic shift after glutamine metabolism inhibition in GLN^{High} cells. **A,** Mitochondrial respiration sustained with glutamine (ΔOCR_{GLN}) after 6 days of EGCG treatment in GBM-1 cells in the absence (black) or presence (gray) of EGCG (110 μmol/L; mean ± SD; $n = 3$; t test). **B,** Mitochondrial respiration sustained with glucose (ΔOCR_{GLC}) after 6 days of EGCG treatment in GBM-1 cells in the absence (black) or presence (gray) of EGCG (110 μmol/L; mean ± SD; $n = 3$; t test). **C,** MPC activity in transfected U87-MG cells with increasing amounts of pyruvate. Cells were transfected with MPC1 + MPC2, grown for 7 days in the presence or absence of EGCG (110 μmol/L) and then BRET was recorded 2 minutes after pyruvate addition (mean ± SD; $n = 3$, two-sided ANOVA). **D,** MPC activity in primary GBM-1 and GBM-10 cells in the absence of pyruvate. Primary cells were transfected with MPC1 + MPC2, grown for 7 days in the presence or absence of 110 μmol/L EGCG (**E**) and then BRET was recorded (mean ± SD; $n = 3$). **E,** Glucose dependency of GBM-1 and GBM-10 cultures. Cell proliferation was assessed using Alamar Blue dye after EGCG treatment (110 μmol/L) for 6 days in the presence of increasing amounts of 2-DG. Results are presented as relative proliferation compared with cells grown in the absence of 2-DG. Each point corresponds to the mean of several experiments ($n \geq 3$; two-sided ANOVA). **F,** Glucose dependency of GLN^{High} and GLN^{Low} cultures. Cell proliferation was assessed as in **E** and 2-DG IC_{50} was extrapolated. Results are presented as relative proliferation compared with control cells grown in the absence of EGCG. Each point corresponds to the mean of 3 experiments (two-sided ANOVA).

concentration in culture media as previously suggested (23). Indeed, glutamine deprivation does not affect proliferation of GLN^{Low} cells even if these cells do use glutamine *in vitro*. Second, our study provides a clear example of tumor heterogeneity in fuel utilization pathways between tumors. Our results are not contradictory with the study by Marin-Valencia and colleagues showing mitochondrial oxidation of glucose rather than glutamine by GBM cells in an orthotopic mice model. Indeed, in their study, they cannot exclude the lack of mesenchymal tumor within the 3 tumors tested because this molecular subtype represents only 30% of the GBM (2, 3, 24). Thus, only a restrictive number of tumors might exhibit an oxidative metabolism supported by glutamine. Finally, our data also validate the use of a fluoro-analogue of glutamine (25) for clinical PET imaging, rather than or in complement to the ^{18}fluoro-2-deoxyglucose (^{18}F-FDG), which capitalizes on enhanced glucose uptake in tumors but is ineffective in evaluating gliomas due to its high background uptake in the brain.

In our study, we showed that GLN^{High} GBM cells are able to generate NADH from a wide variety of oxidizable substrates and as such display a strong metabolic ability to adapt to their microenvironment. These results are in agreement with a recent publication by Jung and colleagues showing that nicotinamide N-methyltransferase (NNMT), involved in NAD utilization and DNA hypomethylation, was consistently upregulated in mesenchymal GBM stem cells (26). In particular, in our study, inhibition of the mitochondrial glutamine supply increases channeling of glycolytic pyruvate into mitochondria. In contrast, GLN^{Low} cells exhibit a strong dependency on glucose associated with a poor survival in the absence of glucose. Metabolic adaptation is especially relevant in solid tumors where metabolic reprogramming is a key determinant allowing cancer cells, including CSC, to survive drastic changes in the tumor microenvironment such as hypoxia, nutrient storage, and acidic pH. In particular, this singular feature of mesenchymal GLN^{High} GBM cells may allow survival in a nutrient-restricted microenvironment as well as a metabolic coupling between tumor cells within a well-oxygenated microenvironment or hypoxic tumor cells. Furthermore, metabolic cross-talk is not restricted to interactions between cancer cells but also extends to a bidirectional metabolic symbiosis

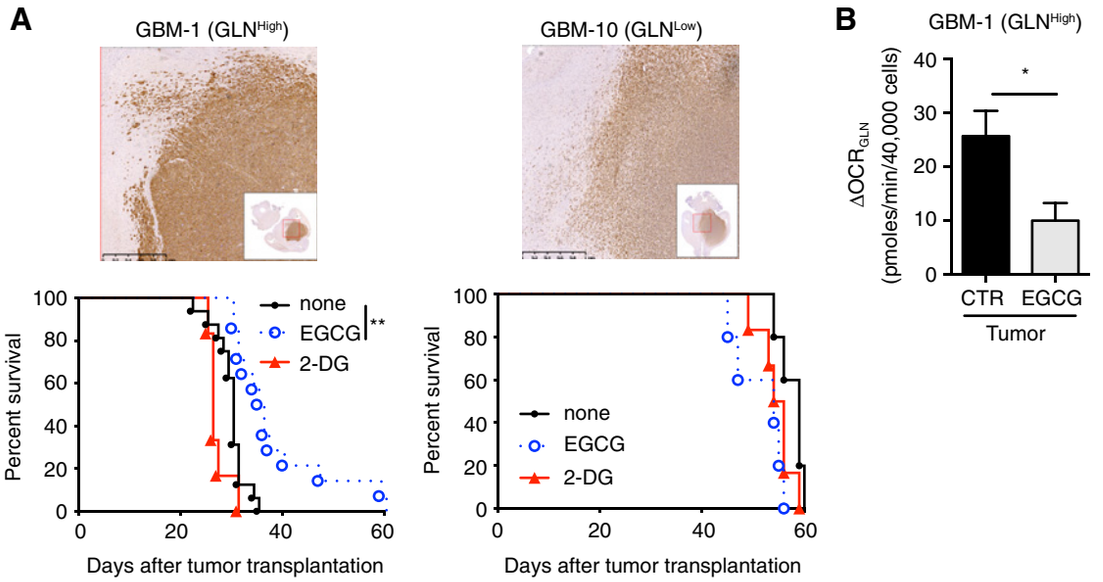

Figure 6.

Glutamine inhibition retards tumor growth *in vivo* in an orthotopic murine model. **A,** Immunohistochemistry of mouse brain injected with control cells using a human–MHC class I antibody (top) and survival curves of mice after orthotopic injection of GLN^{High} (GBM-1, $n = 10$, left) and GLN^{Low} (GBM-10, $n = 5$, right) cultures *in vivo* (bottom). Cells were treated with EGCG (110 μmol/L) for 6 days or 2-DG (5 mmol/L) for 48 hours prior to injection in mouse brain (i.c.). Statistical analyses were performed with the log-rank test compared with control (**, $P < 0.01$). **B,** Mitochondrial respiration sustained with glutamine (ΔOCR_{GLN}) was recorded after injection of glutamine in isolated tumor cells from GBM1-tumor bearing mice. On the day of sacrifice, tumors from mice injected with control or EGCG-pretreated cells were isolated, enriched and ΔOCR_{GLN} was recorded using the Seahorse technology ($n = 2$ in triplicate; *t* test, * $P < 0.05$).

between cancer and stromal cells (27, 28). In fact, Tardito and colleagues recently showed that glutamine required for GBM growth is not supplied by the circulation but rather by astrocytes (8). In this context, alanine, which is highly generated by GLN^{High} cells, could also be used as a carbon source in the TCA cycle following its conversion to pyruvate by other GLN^{High} tumor cells or cells in the microenvironment. This cooperative metabolism coupled to an extensive metabolic plasticity occurring between tumor and stromal cells could be particularly relevant for mesenchymal GLN^{High} GBM cells under nutrient limited conditions and may explain, in part, their very strong aggressiveness.

GBM is an archetype example of a heterogeneous cancer (29) likely underlying the inability of conventional and targeted therapies to achieve long-term remission (30–33). Single-cell RNA sequencing shows that GBM tumors consist of heterogeneous mixtures with individual cells corresponding to different GBM subtypes and this tumor heterogeneity influences clinical outcome (34). Furthermore, these tumors contain CSC adapted to hypoxia and highly resistant to cell death. To overcome the lack of treatment options for GBM, The Cancer Genome Atlas (TCGA) established a comprehensive molecular classification leading to the characterization of four main subtypes, namely, the mesenchymal, classic, neural, and proneural subtypes, based on patient prognosis and distinct genetic, epigenetic and transcriptional alterations (3, 35). Recently, we and others have shown that molecular subtypes of GBM are associated with patient outcome and response to therapy (3, 36). For example, MGMT methylation status is pretty accurate to predict response to temozolomide in the classical subtype but bears little sensitivity in the mesenchymal and proneural subtypes. In our study, we show that the metabolic phenotyping as well as the differential glutamine utilization mirror the molecular classification established by Philips and colleagues and Verhaak and colleagues (2, 3, 37). Furthermore, we show that the pleiotropic metabolic inhibitor EGCG, targeting glutamine metabolism, specifically reduces tumor proliferation, *in vitro* and *in vivo*, of mesenchymal GLN^{High} cells. Surprisingly, the glycolytic inhibitor 2-DG does not improve survival of mice bearing highly glycolytic GLN^{Low} tumors or GLN^{High} cells that shifted their metabolism toward glycolysis after EGCG treatment (data not shown). The absence of *in vivo* effectiveness of 2-DG might be explained by the presence of its natural counterpart glucose, reducing only partially the availability of glucose to tumor cells. In fact, previous publications have shown that whereas 2-DG exhibited cytotoxic effects in cancer cells, administration of 2-DG alone did not lead to significant anticancer activity *in vivo* (38, 39). Thus, metabolic targeting of glutamine metabolism seems a potential pertinent therapeutic strategy, in contrast to glycolysis targeting. These results have several significant fallouts. First, they highlight the complexity of metabolic targeting of tumor cells as both the choice of the metabolic inhibitor and the targeted metabolic pathway are crucial to improve survival outcome. Second, the efficient metabolic inhibition of tumor growth triggered by the mesenchymal GLN^{High} cells is of particular interest because it has been shown that this subtype is the most resistant to therapy (3, 36). Furthermore, a recent study has shown that radiation promotes a molecular shift from the proneural to the mesenchymal subtype (40). In this

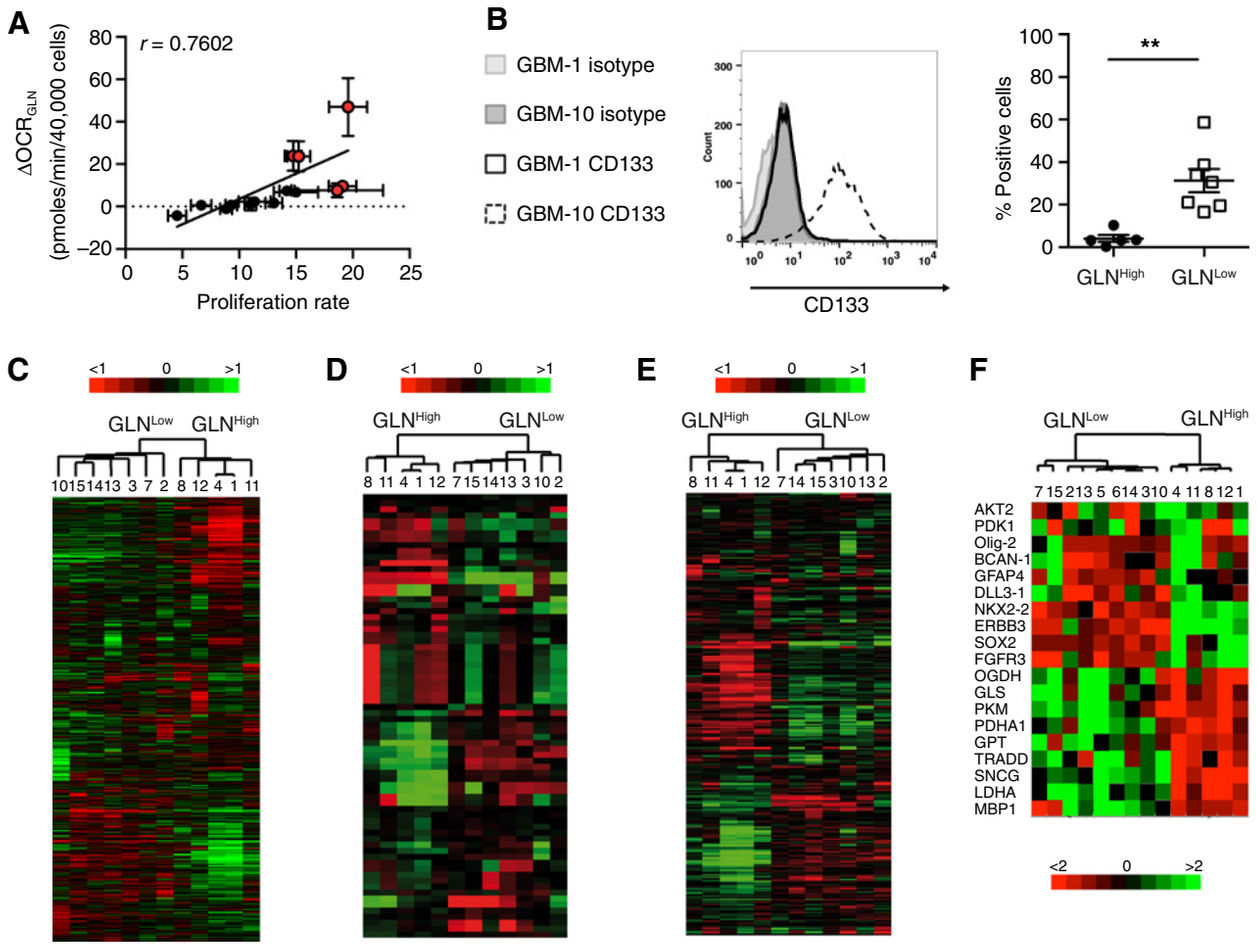

Figure 7.

Phenotypic and molecular features of GLN^{High} cultures. **A,** Correlation between ΔOCR_{GLN} and proliferation of primary GBM cultures. Proliferation was assessed by cell counting using trypan blue exclusion and recorded over 7 days. ΔOCR_{GLN} was calculated as in **2D**. GLN^{High} cultures are indicated in red. **B,** Expression of CD133 assessed by FACS analysis in primary GBM cells. Representative histograms of CD133 expression in GBM-1 (GLN^{High}) and GBM-10 (GLN^{Low}) cultures (left) and dot plot of CD133 expression in GLN^{High} and GLN^{Low} cultures. Each dot represents one primary culture ($n = 5$ GLN^{High} cultures and $n = 7$ GLN^{Low} cultures; mean of 3 experiments; t test, ** $P < 0.01$). **C–E,** Unsupervised hierarchical clustering of 12 primary cultures using transcriptomic analysis using the top 2,000 most variable genes in **C**, the Philips data set probes in **D** and the Verhaak dataset probes in **E**. **F,** Clustering of the 14 primary GBM cultures by RT-qPCR using a subset of genes included among the most discriminant genes. In all heatmaps, low, medium, and high expressions are represented respectively as green, black, and red colors, respectively.

context, it would be interesting to evaluate whereas a metabolic shift occurs with the development of therapeutic resistance, in particular in the proneural GBM subtype. Finally, in the context where the coexistence of genetically divergent tumor subtypes within a tumor has been recently demonstrated (29), a recent study has shown that enrichment in mesenchymal subtype cells within brain tumor was associated with a significantly worse outcome (34). Thus, a therapeutic strategy targeting the most aggressive tumor cells, namely the mesenchymal GLN^{High} cells, should reduce global tumor progression and be advantageous for the patient. Altogether, our results reinforce subtype identification as a fundamental basis for GBM classification and provide a proof of concept of theranostic metabolic targeting opening potential clinical application for a personalized medicine.

In conclusion, the diversity of carbon substrate utilization pathways in tumors is indicative of metabolic heterogeneity that is not only relevant across different cancer types but also within a group of tumors that otherwise share the same diagnosis. Furthermore, our findings provide a functional validation of metabolic targeting associated with molecular signature, prevailing the metabolic plasticity of tumor cells. Thus, further metabolic studies may provide a unique opportunity to evaluate synergistic improvements of actual therapies or designed personalized therapies in GBM, but also in other tumor types.

Disclosure of Potential Conflicts of Interest

No potential conflicts of interest were disclosed.

Authors' Contributions

Conception and design: F.M. Vallette, C. Pecqueur
Development of methodology: C. Chauvin, E. Scotet, V. Compan, C. Pecqueur
Acquisition of data (provided animals, acquired and managed patients, provided facilities, etc.): K. Oizel, C. Chauvin, C. Gratas, F. Geraldo, U. Jarry, E. Scotet, M. Rabe, F. Gautier, D. Loussouarn, C. Pecqueur
Analysis and interpretation of data (e.g., statistical analysis, biostatistics, computational analysis): K. Oizel, C. Chauvin, L. Oliver, C. Gratas, M. Rabe, R. Teusan, F. Gautier, J.-C. Martinou, F.M. Vallette, C. Pecqueur
Writing, review, and/or revision of the manuscript: K. Oizel, C. Chauvin, L. Oliver, C. Gratas, M. Rabe, M.-C. Alves-Guerra, V. Compan, F.M. Vallette, C. Pecqueur
Administrative, technical, or material support (i.e., reporting or organizing data, constructing databases): L. Oliver, F. Geraldo, F.M. Vallette, C. Pecqueur
Study supervision: F.M. Vallette, C. Pecqueur

Acknowledgments

We thank Myriam Robard from the Cellular and Tissular Imaging Core Facility of Nantes University (MicroPICell) for expert technical assistance in the acquisition of imaging data and the human and environmental genomic platform of Rennes. We would like to thank Benoît Vanderperre for providing MPC plasmids. We would like to thank Emeline Brocard, Christian Renaud, Marine Amouriq, and Bryan Caballero for technical help, as well as Jacques Lebreton for providing BPTES. This work was supported by grants from "Ligue contre le cancer," Region Pays de la Loire and LABEX IGO.

The costs of publication of this article were defrayed in part by the payment of page charges. This article must therefore be hereby marked *advertisement* in accordance with 18 U.S.C. Section 1734 solely to indicate this fact.

Received December 9, 2016; revised April 24, 2017; accepted July 13, 2017; published OnlineFirst July 18, 2017.

References

1. Stupp R, Mason WP, van den Bent MJ, Weller M, Fisher B, Taphoorn MJB, et al. Radiotherapy plus concomitant and adjuvant temozolomide for glioblastoma. N Engl J Med 2005;352:987–96.
2. Phillips HS, Kharbanda S, Chen R, Forrest WF, Soriano RH, Wu TD, et al. Molecular subclasses of high-grade glioma predict prognosis, delineate a pattern of disease progression, and resemble stages in neurogenesis. Cancer Cell 2006;9:157–73.
3. Verhaak RGW, Hoadley KA, Purdom E, Wang V, Qi Y, Wilkerson MD, et al. Integrated genomic analysis identifies clinically relevant subtypes of glioblastoma characterized by abnormalities in PDGFRA, IDH1, EGFR, and NF1. Cancer Cell 2010;17:98–110.
4. Brennan CW, Verhaak RGW, McKenna A, Campos B, Noushmehr H, Salama SR, et al. The somatic genomic landscape of glioblastoma. Cell 2013;155:462–77.
5. Morfouace M, Lalier L, Bahut M, Bonnamain V, Naveilhan P, Guette C, et al. Comparison of spheroids formed by rat glioma stem cells and neural stem cells reveals differences in glucose metabolism and promising therapeutic applications. J Biol Chem 2012;287:33664–74.
6. Hanahan D, Weinberg RA. Hallmarks of cancer: the next generation. Cell 2011;144:646–74.
7. Hensley CT, Faubert B, Yuan Q, Lev-Cohain N, Jin E, Kim J, et al. Metabolic Heterogeneity in Human Lung Tumors. Cell 2016;164:681–94.
8. Tardito S, Oudin A, Ahmed SU, Fack F, Keunen O, Zheng L, et al. Glutamine synthetase activity fuels nucleotide biosynthesis and supports growth of glutamine-restricted glioblastoma. Nat Cell Biol 2015;17:1556–68.
9. Lyssiotis CA, Son J, Cantley LC, Kimmelman AC. Pancreatic cancers rely on a novel glutamine metabolism pathway to maintain redox balance. Cell Cycle 2013;12:1987–8.
10. Marin-Valencia I, Yang C, Mashimo T, Cho S, Baek H, Yang X-L, et al. Analysis of tumor metabolism reveals mitochondrial glucose oxidation in genetically diverse human glioblastomas in the mouse brain in vivo. Cell Metab 2012;15:827–37.
11. Palm W, Park Y, Wright K, Pavlova NN, Tuveson DA, Thompson CB. The utilization of extracellular proteins as nutrients is suppressed by mTORC1. Cell 2015;162:259–70.
12. Porporato PE, Payen VL, Pérez-Escuredo J, De Saedeleer CJ, Danhier P, Copetti T, et al. A mitochondrial switch promotes tumor metastasis. Cell Rep 2014;8:754–66.
13. Caro P, Kishan AU, Norberg E, Stanley IA, Chapuy B, Ficarro SB, et al. Metabolic signatures uncover distinct targets in molecular subsets of diffuse large B cell lymphoma. Cancer Cell 2012;22:547–60.
14. Gross MI, Demo SD, Dennison JB, Chen L, Chernov-Rogan T, Goyal B, et al. Antitumor activity of the glutaminase inhibitor CB-839 in triple-negative breast cancer. Mol Cancer Ther 2014;13:890–901.
15. de Hoon MJL, Imoto S, Nolan J, Miyano S. Open source clustering software. Bioinforma Oxf Engl 2004;20:1453–4.
16. Zeeberg BR, Feng W, Wang G, Wang MD, Fojo AT, Sunshine M, et al. GoMiner: a resource for biological interpretation of genomic and proteomic data. Genome Biol 2003;4:R28.
17. Ashburner M, Ball CA, Blake JA, Botstein D, Butler H, Cherry JM, et al. Gene ontology: tool for the unification of biology. The Gene Ontology Consortium. Nat Genet 2000;25:25–9.
18. Bochner BR, Siri M, Huang RH, Noble S, Lei X-H, Clemons PA, et al. Assay of the multiple energy-producing pathways of mammalian cells. PLoS One 2011;6:e18147.
19. Gratas C, Séry Q, Rabé M, Oliver L, Vallette FM. Bak and Mcl-1 are essential for Temozolomide induced cell death in human glioma. Oncotarget 2014;5:2428–35.
20. Compan V, Pierredon S, Vanderperre B, Krznar P, Marchiq I, Zamboni N, et al. Monitoring mitochondrial pyruvate carrier activity in real time using a BRET-based biosensor: investigation of the Warburg effect. Mol Cell 2015;59:491–501.
21. Pavlova NN, Thompson CB. The emerging hallmarks of cancer metabolism. Cell Metab 2016;23:27–47.
22. Rossignol R, Gilkerson R, Aggeler R, Yamagata K, Remington SJ, Capaldi RA. Energy substrate modulates mitochondrial structure and oxidative capacity in cancer cells. Cancer Res 2004;64:985–93.
23. Davidson SM, Papagiannakopoulos T, Olenchock BA, Heyman JE, Keibler MA, Luengo A, et al. Environment impacts the metabolic dependencies of Ras-driven non-small cell lung cancer. Cell Metab 2016;23:517–28.
24. Kim Y-W, Koul D, Kim SH, Lucio-Eterovic AK, Freire PR, Yao J, et al. Identification of prognostic gene signatures of glioblastoma: a study based on TCGA data analysis. Neuro-Oncol 2013;15:829–39.
25. Venneti S, Dunphy MP, Zhang H, Pitter KL, Zanzonico P, Campos C, et al. Glutamine-based PET imaging facilitates enhanced metabolic evaluation of gliomas in vivo. Sci Transl Med 2015;7:274ra17.
26. Jung J, Kim LJY, Wang X, Wu Q, Sanvoranart T, Hubert CG, et al. Nicotinamide metabolism regulates glioblastoma stem cell maintenance. JCI Insight 2017;2.
27. Pavlides S, Whitaker-Menezes D, Castello-Cros R, Flomenberg N, Witkiewicz AK, Frank PG, et al. The reverse Warburg effect: aerobic glycolysis in cancer associated fibroblasts and the tumor stroma. Cell Cycle Georget Tex 2009;8:3984–4001.
28. Quail DF, Joyce JA. Microenvironmental regulation of tumor progression and metastasis. Nat Med 2013;19:1423–37.
29. Sottoriva A, Spiteri I, Piccirillo SGM, Touloumis A, Collins VP, Marioni JC, et al. Intratumor heterogeneity in human glioblastoma reflects cancer evolutionary dynamics. Proc Natl Acad Sci U S A 2013;110:4009–14.
30. Nathanson DA, Gini B, Mottahedeh J, Visnyei K, Koga T, Gomez G, et al. Targeted therapy resistance mediated by dynamic regulation of extrachromosomal mutant EGFR DNA. Science 2014;343:72–6.
31. Gilbert MR, Dignam JJ, Armstrong TS, Wefel JS, Blumenthal DT, Vogelbaum MA, et al. A randomized trial of bevacizumab for newly diagnosed glioblastoma. N Engl J Med 2014;370:699–708.
32. Stommel JM, Kimmelman AC, Ying H, Nabioullin R, Ponugoti AH, Wiedemeyer R, et al. Coactivation of receptor tyrosine kinases affects the response of tumor cells to targeted therapies. Science 2007;318:287–90.

33. Chen J, Li Y, Yu T-S, McKay RM, Burns DK, Kernie SG, et al. A restricted cell population propagates glioblastoma growth after chemotherapy. Nature 2012;488:522–6.
34. Patel AP, Tirosh I, Trombetta JJ, Shalek AK, Gillespie SM, Wakimoto H, et al. Single-cell RNA-seq highlights intratumoral heterogeneity in primary glioblastoma. Science 2014;344:1396–401.
35. Noushmehr H, Weisenberger DJ, Diefes K, Phillips HS, Pujara K, Berman BP, et al. Identification of a CpG island methylator phenotype that defines a distinct subgroup of glioma. Cancer Cell 2010; 17:510–22.
36. Ducray F, de Reyniès A, Chinot O, Idbaih A, Figarella-Branger D, Colin C, et al. An ANOCEF genomic and transcriptomic microarray study of the response to radiotherapy or to alkylating first-line chemotherapy in glioblastoma patients. Mol Cancer 2010;9:234.
37. Verhaak RGW. Moving the needle: optimizing classification for glioma. Sci Transl Med 2016;8:350fs14.
38. Maher JC, Krishan A, Lampidis TJ. Greater cell cycle inhibition and cytotoxicity induced by 2-deoxy-D-glucose in tumor cells treated under hypoxic vs. aerobic conditions. Cancer Chemother Pharmacol 2004;53: 116–22.
39. Maschek G, Savaraj N, Priebe W, Braunschweiger P, Hamilton K, Tidmarsh GF, et al. 2-deoxy-D-glucose increases the efficacy of adriamycin and paclitaxel in human osteosarcoma and non-small cell lung cancers in vivo. Cancer Res 2004;64:31–4.
40. Halliday J, Helmy K, Pattwell SS, Pitter KL, LaPlant Q, Ozawa T, et al. In vivo radiation response of proneural glioma characterized by protective p53 transcriptional program and proneural-mesenchymal shift. Proc Natl Acad Sci U S A 2014;111:5248–53.